ADVANCED SUSTAINABLE SYSTEMS
www.advsustainsys.com

Cyanobacterial Artificial Plants for Enhanced Indoor Carbon Capture and Utilization

*Maryam Rezaie and Seokheun Choi**

Indoor carbon dioxide (CO_2) levels are often significantly higher than those outdoors, which is a growing health concern, particularly in urban areas where people spend over 80% of their time indoors. Traditional CO_2 mitigation methods, such as ventilation and filtration, are becoming less effective as outdoor CO_2 levels increase due to global warming. This study introduces a novel solution: cyanobacterial artificial plants that enhance indoor carbon capture while converting CO_2 into oxygen (O_2) and bioelectricity. These artificial plants use indoor light to drive photosynthesis, achieving a 90% reduction in indoor CO_2 levels, from 5000 to 500 ppm—far surpassing the 10% reduction seen with natural plants. In addition to improving air quality, the system produces O_2 and enough bioelectricity to power portable electronics. Each artificial leaf contains five biological solar cells that generate electricity during photosynthesis, with water and nutrients supplied through transpiration and capillary action, mimicking natural plant systems. The system generates an open circuit voltage of 2.7 V and a maximum power output of 140 µW. This decentralized approach offers a sustainable, energy-efficient solution to indoor environmental challenges, providing improved air quality and renewable electricity amid rising global CO_2 levels.

1. Introduction

The World Health Organization (WHO) has designated poor air quality as the foremost environmental threat to public health worldwide.[1] It is alarming that 90% of people globally are exposed to air that does not meet the WHO's recommended quality standards. Indoor air quality is often significantly poorer than outdoor air quality because of persistent pollution sources within buildings.[1,2] Those sources include materials used in construction and household products, as well as human activities such as cooking, heating, and cleaning.[3] Additionally, the human metabolism contributes to indoor pollution, particularly in tightly sealed environments designed to maintain stable indoor temperatures.[4] With most people now spending more than 80% of their time indoors, both the duration and intensity of exposure to poor air quality have markedly increased.[1–3] Furthermore, the COVID-19 pandemic has underscored the critical importance of maintaining good indoor air quality.[5] Identified indoor air pollutants encompass a wide range of substances, including particulate matter, biological organisms, allergens, and organic and inorganic chemical compounds.[1–3] Additionally, various reactive chemicals such as ozone and sulfur dioxide are present.[1]

Among various air pollutants, carbon dioxide (CO_2) stands out as the primary greenhouse gas, contributing to 80% of all human-caused climate-changing emissions globally.[1,2] Additionally, as CO_2 levels typically correlate with the presence of other pollutants, they are often used as an indicator of indoor air quality.[6] However, CO_2 is a direct indoor pollutant that threatens human health.[1,2,4] Elevated concentrations ranging from 1000 to 3000 parts per million (ppm), even for just a few hours, can significantly impair cognition and decision-making.[2] Exposure levels of 2000 to 4,000 ppm for several hours can trigger inflammatory responses and lead to health issues such as headaches, drowsiness, and fatigue.[1] Chronic exposure to very elevated levels of CO_2 may result in more severe conditions including bone demineralization, kidney calcification, obesity, and in extreme cases, respiratory failure and loss of consciousness.[2,4] Several regulations and standards define acceptable CO_2 concentrations to ensure indoor air quality. For example, the European Standard recommends a maximum of 800 ppm, while countries such as France, the U.K., and Portugal typically accept an average concentration of 1,000 ppm.[1,2] The American Society of Heating also uses 1,000 ppm as a benchmark, making it a common threshold.[1] Despite the guidelines, studies frequently report that CO_2 levels in indoor environments such as schools, offices,

M. Rezaie, S. Choi
Bioelectronics & Microsystems Laboratory
Department of Electrical & Computer Engineering
State University of New York at Binghamton
Binghamton, NY 13902, USA
E-mail: sechoi@binghamton.edu
S. Choi
Center for Research in Advanced Sensing Technologies & Environmental Sustainability
State University of New York at Binghamton
Binghamton, NY 13902, USA

The ORCID identification number(s) for the author(s) of this article can be found under https://doi.org/10.1002/adsu.202400401

DOI: 10.1002/adsu.202400401

and underground transportation often exceed 2,500 ppm, with peaks sometimes surpassing 5,000 ppm.[1,6]

Carbon capture and storage (CCS) technology has become a crucial research focus in the 21st century, aimed at capturing CO_2 emissions from fossil fuels and securely storing them.[7–9] Despite their promise, that technology has been met with skepticism because of the significant financial investment and energy required for the separation, transportation, and storage of CO_2, coupled with uncertainties about the permanence of storage. Consequently, there has been a shift toward carbon capture and utilization (CCU) technology, where captured CO_2 is converted into high-value products or chemicals through methods such as thermochemical, biochemical, photochemical, and electrochemical processes.[1,9–11] The new approach reduces emissions and harnesses CO_2 as a renewable resource for energy and resource recovery. However, CCS and CCU are primarily focused on large-scale outdoor CO_2 emissions and have not been effectively adapted for indoor CO_2 management because of their great expense and substantial space and energy requirements.

The most common, albeit passive, method for controlling indoor CO_2 levels involves manually opening windows or operating building ventilation systems to equalize indoor and outdoor CO_2 concentrations.[2] While these approaches have been widely used to improve indoor air quality, they are inefficient for precisely controlling CO_2 levels and are becoming less effective as outdoor air quality deteriorates as humans pump more global-warming gases into the atmosphere. A more active and reliable alternative involves integrating filters or sorbent materials into ventilation systems, similar to outdoor CCS techniques but designed for temporary CO_2 containment.[1–3,12] However, once these materials become saturated, they require replacement or the captured CO_2 needs to be released. This cycle escalates costs, reduces air quality efficiency, and may increase outdoor CO_2 emissions. The most economical and environmentally friendly method uses houseplants, which naturally absorb CO_2 and release oxygen (O_2).[13–16] That strategy mirrors large-scale outdoor CCU techniques that use the natural carbon cycle to convert captured CO_2 into beneficial compounds, thus sustainably improving air quality. Additionally, indoor plants help purify the air by eliminating other pollutants and airborne microbes, while effectively regulating indoor humidity levels.[13,14] However, this approach is constrained by its substantial maintenance demands, which are time-intensive and costly. Furthermore, the presence of indoor plants can increase pollen levels and potential allergenicity, often accompanied by strong fragrances.[3] Challenges such as the need for regular maintenance, coupled with their slow growth and gas exchange rates, hinder the practical implementation of houseplants in indoor environments. Additionally, the limited portability of houseplants and their requirement for specific environmental conditions render them less suitable as a widespread decentralized system for managing indoor air quality.

In this study, we introduce a groundbreaking artificial plant that harnesses cyanobacterial CO_2 fixation to generate oxygen and bioelectricity during their photosynthesis, acting as a miniaturized version of CCU technology tailored for indoor environments (**Figure 1a**). This system is designed to be compact, requiring minimal space and maintenance, while offering significantly faster growth and gas exchange rates sustainably. The artificial plant uses indoor light to enable cyanobacteria to convert CO_2 and water into oxygen, thereby improving indoor air quality (Figure 1b). This system features artificial leaves, each containing five biological solar cells (called biosolar cells) (Figure 1c). A single biosolar cell comprises a cyanobacteria-infused anode, a cathode, and an ion exchange membrane (Figure 1d). These cells are interconnected electrically, via metallic paths, and fluidically, through a microfluidic channel. The selected cyanobacteria, *Synechocystis* sp. PCC 6803, is known for its exoelectrogenic properties,[17,18] enabling it to produce bioelectricity during photosynthesis. Transpiration and capillary action bring water and nutrients to each biosolar cell, mimicking the nutrient distribution systems in living plants and trees. A porous anode effectively captures CO_2 molecules and it is decorated with iron oxide nanoparticles (Fe_2O_3 NPs) to enhance light capture and electrocatalytic activity. Additionally, the cathodic function is augmented by a coating of palladium nanoparticles (Pd NPs). Our innovative integration of material science and biological entities presents a very promising solution for the simultaneous capture and utilization of CO_2. This approach offers a valuable decentralized system for enhancing indoor air quality and generating electricity.

2. Results and Discussion

2.1. Design and Structure of Artificial Plants, Leaves, and Integrated Biosolar cells

As shown in Figures S1 and S2 (Supporting Information), a 1.6 mm-thick poly(methyl methacrylate) (PMMA) plant scaffold was crafted using a precision laser cutting technique. The PMMA structure was designed to incorporate five leaves, each embedded with five biosolar cells (Figures 1a,b). The biosolar cells comprised a cyanobacteria-infused anode, an ion-exchange membrane, and a cathode (Figures 1c,d). Initially, the PMMA scaffold was engraved with fluidic and electrical channels. Subsequently, specific areas were further engraved to accommodate the biosolar cells. Materials essential for the biosolar cells' functionality were systematically introduced into these areas. Hygroscopic materials were integrated into the fluidic branches and trunk to facilitate the absorption of water and nutrients through capillary action and transpiration. Concurrently, electrical channels were embedded with conductive silver paste to ensure efficient conductivity. This intricate assembly was achieved using our well-established inkjet printing technique.[19,20] To optimize the system's functionality, all anodes across the leaves were interconnected fluidically via branches extending from the main trunk. Meanwhile, the biosolar cells within each leaf were wired in series, and all five leaves were interconnected in series to enhance the overall energy efficiency and distribution. The assembled plant-like scaffold can be placed into a soil-containing pot, much like a conventional plant (Figures 1a,b). This arrangement allows for the continuous supply of water and nutrients, essential for supporting the growth and metabolic functions of the cyanobacteria within the biosolar cells. When placed indoors, the plant-like structure in the pot uses indoor lighting and ambient CO_2, along with supplied water, to facilitate the photosynthetic process of the cyanobacteria. This process converts CO_2 into O_2, effectively serving as a carbon capture

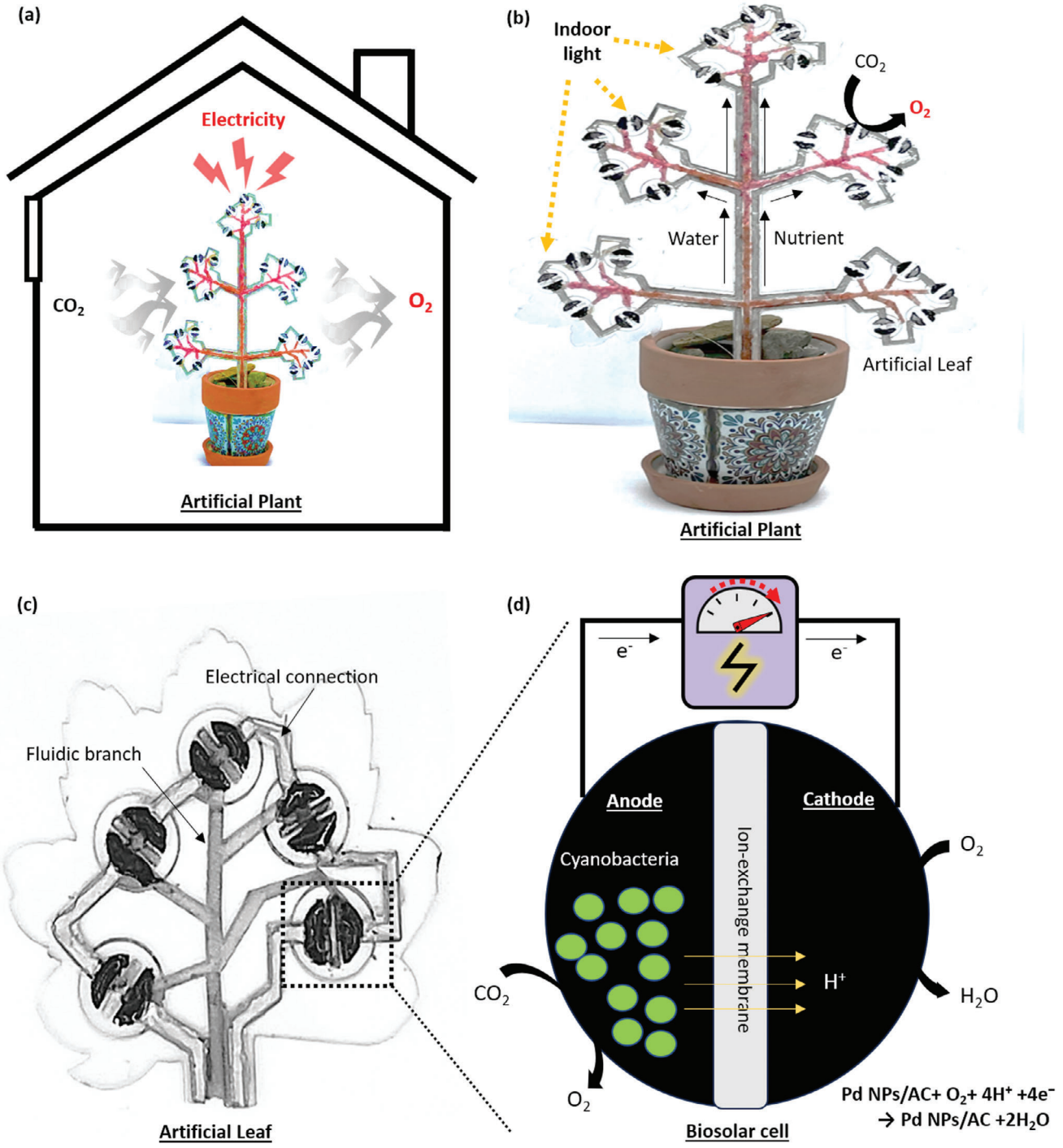

Figure 1. Operating principle of cyanobacterial artificial plants for indoor carbon capture and utilization. a) An artificial plant converting captured CO_2 into O_2 and bioelectricity during photosynthesis. b) An artificial plant utilizing indoor light, water, and nutrients to convert CO_2 into O_2, thereby enhancing indoor air quality. c) A photograph of the artificial leaf of the plant, showing five biosolar cells attached to a stem. The cells are electrically connected outside the stem, which transports fluids. d) A schematic illustration of the biosolar cell, consisting of a cyanobacteria-infused anode, a cathode, and an ion exchange membrane. The electrogenic cyanobacteria generate electricity during photosynthesis. (AC: Activated carbon).

and utilization pathway, transforming indoor greenhouse gases into breathable oxygen. During photosynthesis, cyanobacteria generate excess electrons through the bacterial photosynthetic electron transfer process, which are then transported extracellularly to the anode.[17,18] This transfer creates an electrical current, providing an alternative route for carbon utilization. Simultaneously, protons produced alongside the electrons during photosynthesis are selectively transported through the ion exchange membrane to the cathode. Finally, they react with atmospheric O_2 to complete the cathodic reaction. This crucial process is essential for maintaining the electroneutrality of the system. It is important to highlight that cyanobacterial metabolism relies on the respiration of O_2 present in the air, while the cathodic reaction in the biosolar cell also requires O_2. Nonetheless, the O_2 produced by photosynthesis exceeds the amount consumed by these processes, leading to a net increase in the available oxygen. This will be explored in the final chapter of this manuscript.

2.2. Design and Characterization of Anodic and Cathodic Materials

To enhance the practicality of the cyanobacterial artificial plant for indoor carbon capture and utilization, significant advancements were made in the materials and designs of the biosolar cell. The anode materials and their architectural configurations are particularly crucial, profoundly influencing the overall performance. These improvements affect several key areas: (i) porosity, which facilitates gas exchange, product removal, and fluid absorption via transpiration; (ii) the surface area available for cyanobacterial attachment; (iii) the efficiency of light absorption and its conversion to electricity; and (iv) the efficiency of extracellular electron transfer. Our anode replicates the three-dimensional porous structure of natural leaves, complete with minuscule pores akin to stomata. The structure is pivotal for the effective exchange of gases and the release of water vapor through transpiration. By treating graphene oxide (GO) with an iron nitrate solution via a hydrothermal process, we created a reduced graphene oxide (rGO) hydrogel embedded with iron oxide nanoparticles (Fe_2O_3 NPs).

This very conductive, porous architecture facilitates efficient gas exchange and provides an extensive surface area for cyanobacterial colonization (Figure S3, Supporting Information) and effective removal of bacterial byproducts, thereby enhancing the capture and conversion of CO_2 to O_2. Notably, the nanoparticles act as potent light absorbers, which enhances light harvesting, and electrical conduits, which improve electron transfer from bacterial photosynthesis, thus boosting carbon utilization and electricity generation. The scanning electron microscopy (SEM) image shown in **Figure 2a** illustrates the very porous structure and interconnected lattice morphology characteristic of our NP-decorated rGO hydrogel anode. Energy Dispersive X-ray (EDX) microanalysis, as shown in Figure 2b, confirms the presence of carbon, oxygen, and iron elements, with iron distribution being particularly delineated through mapping analysis. X-ray Photoelectron Spectroscopy (XPS) results, presented in Figure 2c, verify the presence of these elements through distinct spectral peaks. Notably, iron exhibits binding energy peaks ranging from 706 to 723 eV for Fe2p orbitals, which vary according to its oxidation state. GO, meanwhile, is marked by a prominent peak at 532 eV; this peak notably diminishes in intensity following the reduction process of the material, indicating a decrease in oxygen content.[21] Cyclic voltammetry (CV) measurements, conducted in a three-electrode electrochemical cell with a scan rate of 100 mV s^{-1}, are detailed in Figure 2d. These measurements reveal significant electrochemical activity in the NP-enhanced rGO hydrogel compared to both GO and rGO alone. The enhanced electrochemical performance of the rGO hydrogel over the GO hydrogel is attributable to increased electrical conductivity and improved charge transfer capabilities, arising from the removal of oxygen-containing functional groups, as evidenced by Electrochemical Impedance Spectroscopy (EIS) results (Inset of Figure 2d).

Furthermore, the incorporation of Fe_2O_3 NPs into the rGO hydrogel substantially augments the electrocatalytic activity, demonstrated by marked reduction and oxidation peaks in the CV profile at potentials of + 0.72 and –0.62 V, respectively. The Fe_2O_3 NPs promote electron transfer and enhance the rate of redox reactions, crucial for effective electrocatalysis, as shown in the inset of Figure 2d.[22] This integration of Fe_2O_3 NPs not only improves the electrochemical properties of the hydrogel but underscores its potential in advanced energy-producing applications. The UV–vis spectroscopic analysis, as illustrated in Figure 2e, highlights the enhanced light use and photocatalytic activity of our cyanobacteria-embedded anode. This analysis indicates that the anode retains the characteristic absorption peaks of cyanobacteria alone but exhibits increased transmittance. The elevated transmittance levels are critical for optimizing light capture, while the inherent absorption capabilities of the material facilitate efficient photon harvesting essential for photocatalytic processes. This synergistic interaction between the cyanobacteria and our improved anode's matrix not only maximizes light absorption but also effectively utilizes this energy in the photocatalytic conversion of CO_2 into valuable products such as O_2 and bioelectricity. During the photosynthetic process of the cyanobacteria, this capability is crucial for reducing atmospheric CO_2 levels.

The performance of the biosolar cell is significantly influenced by the characteristics of the cathode compartment. This compartment necessitates electron acceptors to facilitate the redox processes, as electrons and protons are transported from the anode to maintain the charge neutrality of the cell. In this study, an air-cathode was employed because of the advantages of oxygen, which is abundantly available, sustainable, and biocompatible.[23] Although there is competition for O_2 between the cathodic reactions and cyanobacterial respiration—which can diminish O_2 production and potentially affect indoor air quality—the consumption of O_2 remains considerably low. Furthermore, the amount of O_2 generated by photosynthesis substantially exceeds that consumed by the cathodic reactions and bacterial respiration, underscoring the efficiency of the biosolar cell in using this electron acceptor. To enhance O_2 absorption from the air, a novel porous structure using activated carbon (AC) hydrogel was engineered (**Figure 3a**).[24] The efficiency of the oxygen reduction reaction was significantly augmented by the integration of a highly active palladium (Pd) nanoparticle (NP) catalyst within the AC hydrogel. This addition markedly improved the reaction kinetics,

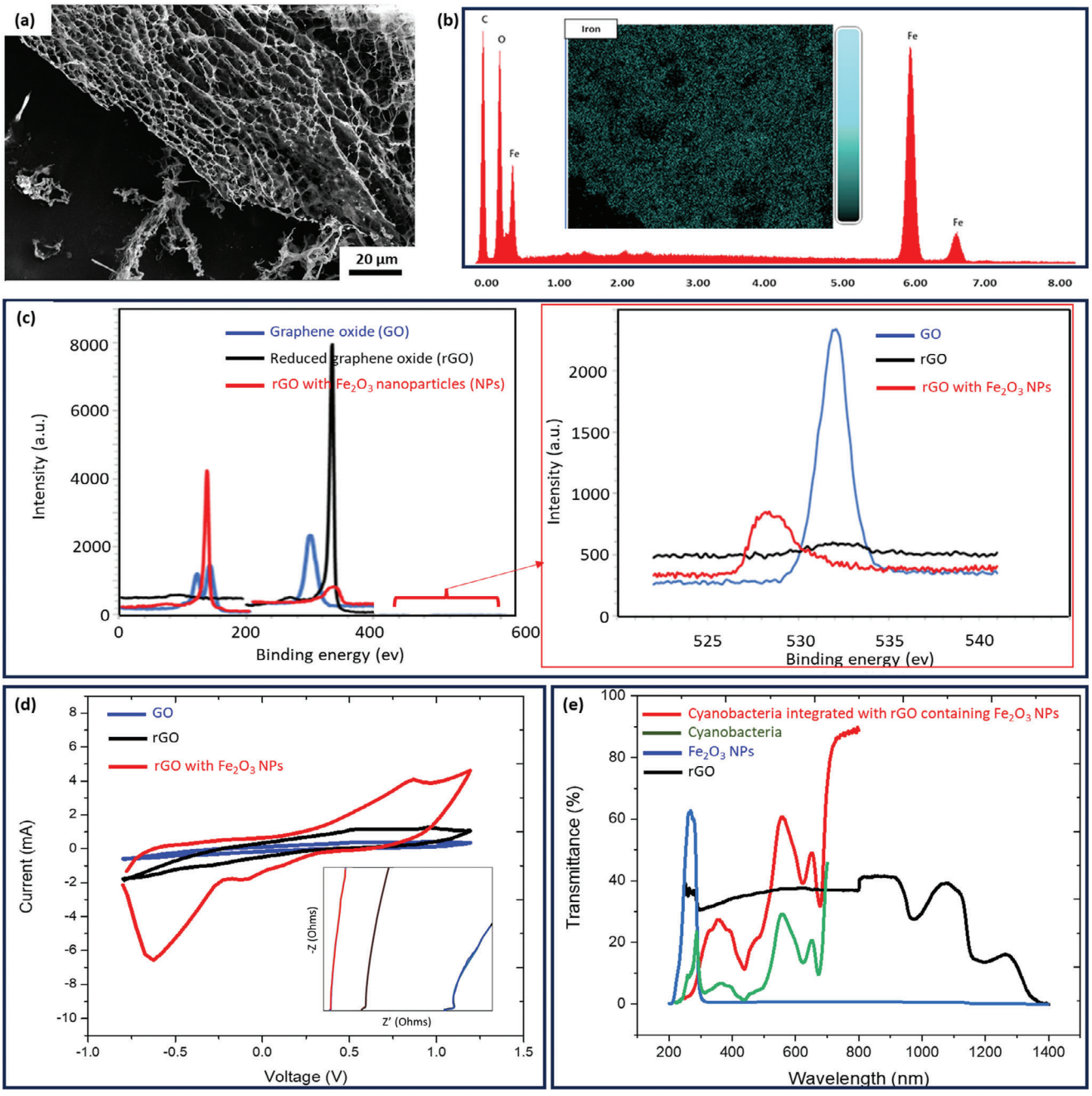

Figure 2. Structure and characterization of the Fe_2O_3 NPs-decorated rGO hydrogel anode in the biosolar cell. a) SEM image of the anode displaying its porosity. b) EDX spectrum and mapping revealing the presence and uniform distribution of Fe_2O_3 NPs. c) XPS survey spectra of different hydrogel samples; graphene oxide (GO), reduced graphene oxide (rGO), and rGO with Fe_2O_3 nanoparticles (NPs). d) CV profiles for those hydrogel samples (inset: EIS profiles). e) Transmittance spectra obtained by UV–vis spectroscopy of rGO, Fe_2O_3 NPS, cyanobacteria, and cyanobacteria integrated into the rGO hydrogel decorated with Fe_2O_3 NPS.

leading to an accelerated rate of the oxygen reduction reaction. Electrochemical analyses, including CV and linear sweep voltammetry (LSV), shown in Figures 3b,c respectively, demonstrated improved electrochemical reactions. Additionally, the EIS profile revealed a substantially enhanced electron transfer efficiency, evidenced by the reduced impedance at the interface between the NP-decorated hydrogel and the electrolyte (Figure 3d).

The integration of these functional attributes distinctly positions our anode and cathode materials as highly effective catalysts in environmental remediation strategies, particularly tailored for enhancing indoor air quality. By facilitating the conversion of CO_2 into O_2 and bioelectricity, these materials contribute to reducing CO_2 levels and generate valuable byproducts that can be utilized in various applications.

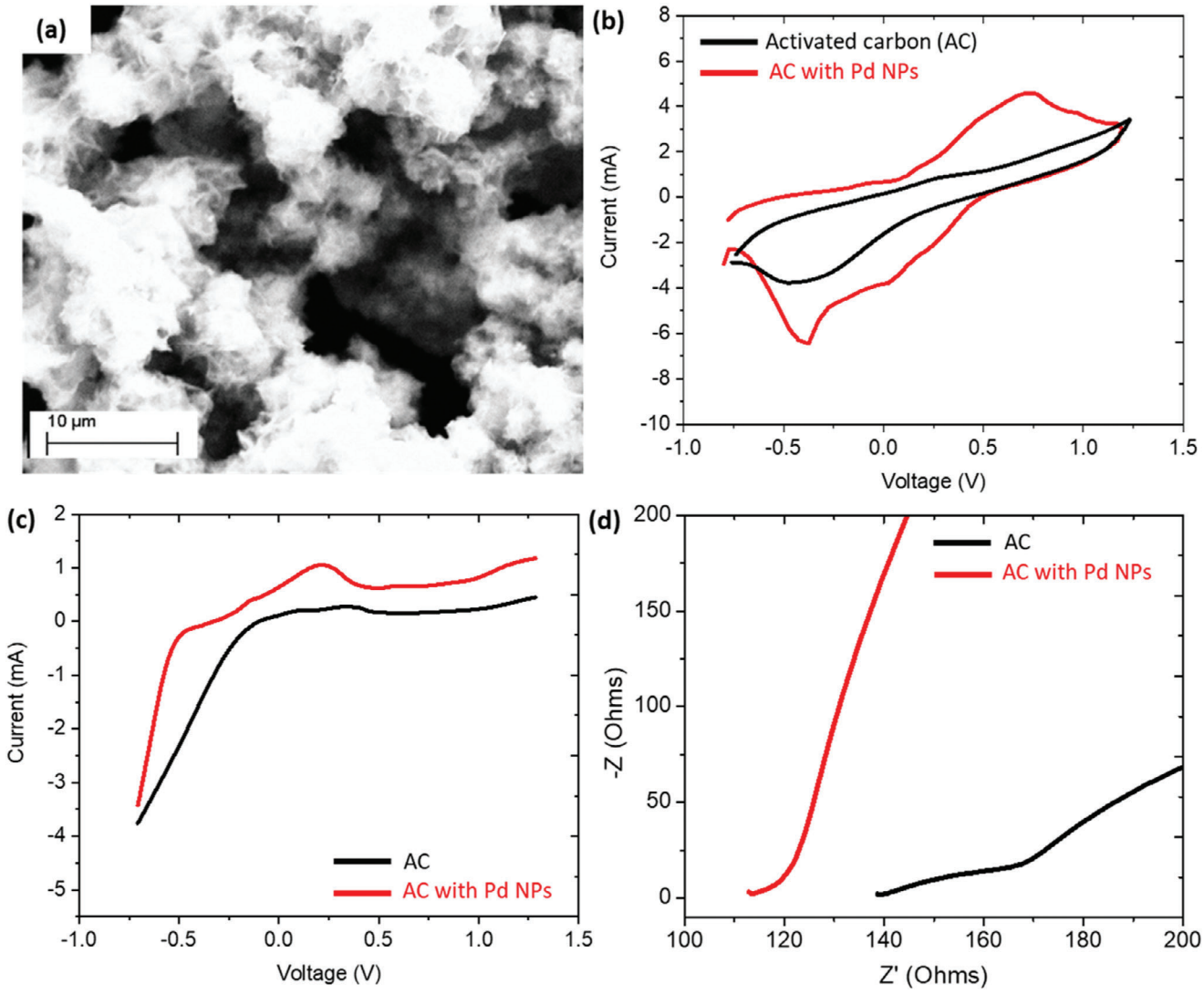

Figure 3. Structure and characterization of the Pd NPs-decorated AC hydrogel cathode in the biosolar cell. a) SEM image of the cathode displaying its porosity. b) CV, c) LSV, and d) EIS of the cathode with and without Pd NPs.

2.3. Enhanced Nutrient and Water Supply Management for Sustained Operation

The fundamental unit of the artificial plant, the biosolar cell, is theoretically self-sustaining.[17,18] In this system, cyanobacteria use light, water, and CO_2 to perform photosynthesis, generating O_2 and organic matter. These products are then used in their respiration processes, recycling CO_2 and water, thereby forming a closed-loop cycle. This makes the biosolar cell a promising self-sustainable power solution. However, practical applications face challenges because of the cell's limited lifespan. In a closed system, essential nutrients required for bacterial growth, metabolism, and photosynthesis, such as phosphorus, are not inherently replenished.[25,26] Typically, living plants absorb these nutrients from their environment as they are dissolved in water. This discrepancy highlights a significant hurdle in achieving true self-sustainability for biosolar cells in real-world conditions. In this study, individual biosolar cells, each containing a hygroscopic freeze-dried hydrogel anode, were fluidically interconnected through branches that extended from a central trunk. To enhance the management of water and nutrient supply from the base, where these resources were introduced, the branches and trunk were filled with a hygroscopic gelatin-chitosan hydrogel.[27] This composite hydrogel features crosslinked polymer networks, which provide outstanding water absorption capabilities and facilitate molecular diffusion. These properties are primarily attributed to the presence of hydrophilic functional groups, such as amino and hydroxyl groups, within the polymer structure. This innovative design significantly improves the efficiency of resource distribution throughout the biosolar cell system. Here, the management of water and nutrient supply was engineered to emulate natural plant processes through two primary mechanisms: transpiration and capillary action, as illustrated in **Figure 4a**.[28] Transpiration involves the evaporation of water from the leaf surface, aiding in nutrient transport and cooling. Capillary action, on the other hand, relies on the forces of adhesion, cohesion,

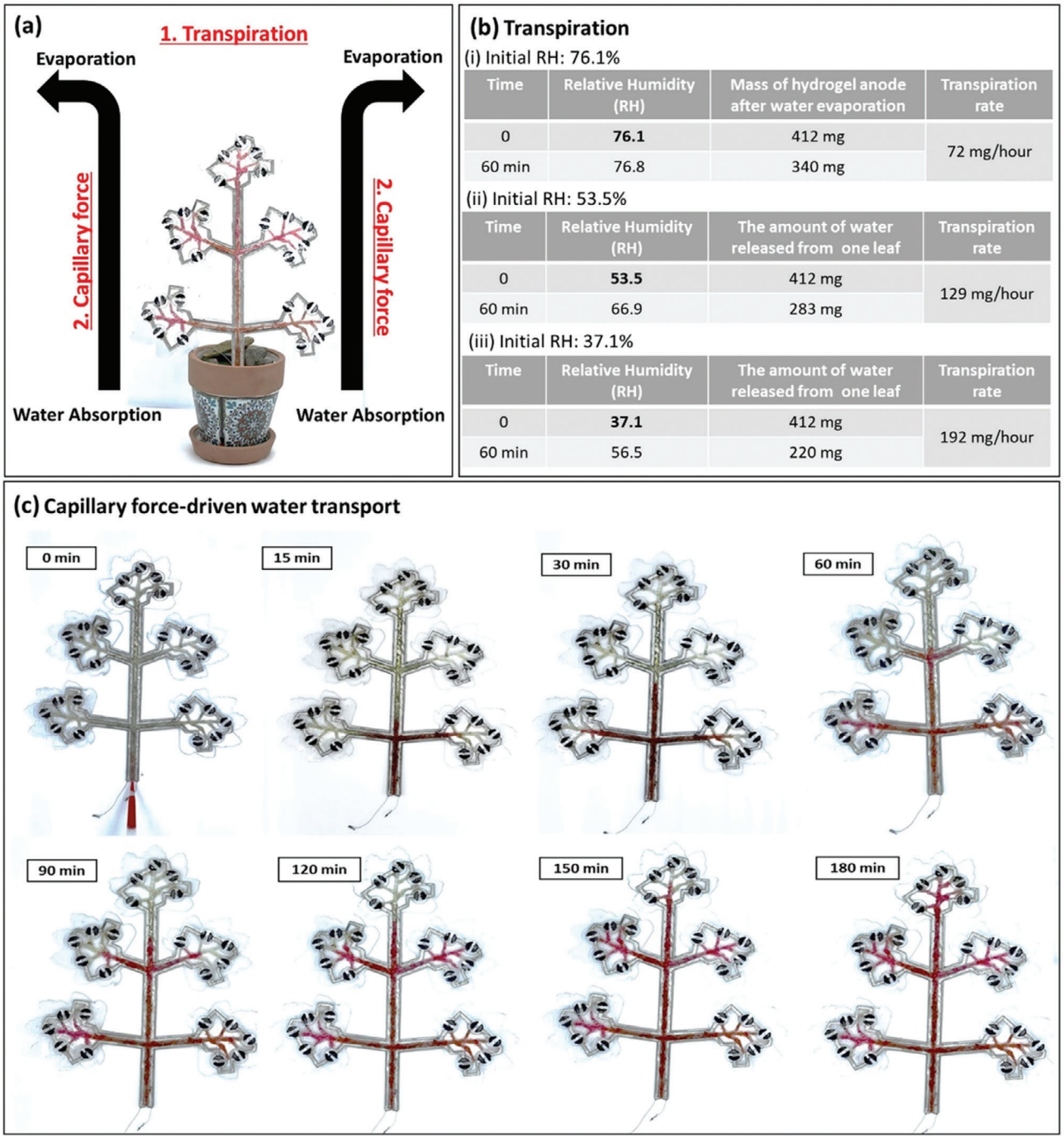

Figure 4. Mechanism for nutrient and water supply management. a) Two mechanisms: transpiration and capillary action. b) Transpiration rate of the hydrogel anode. c) Time-lapse images showing capillary action-driven flow of red ink through the artificial plant.

and surface tension within narrow spaces to move water upward. However, because of gravitational forces, capillary action alone may sometimes be inadequate for transporting water to the upper parts of the plant. In these instances, transpiration provides an additional driving force, enhancing the upward movement of water and nutrients.[29] Initially, the transpiration capabilities of the hygroscopic hydrogel anode, simulating the leaf surface where evaporation occurs, were evaluated under varying conditions of relative humidity (RH) (Figure 4b). At a high RH of 76.1%, the fully saturated hydrogel anode exhibited slow evaporation rates, releasing ≈72 mg of water per hour. As the RH decreased to 53.5%, the rate of transpiration increased to 129 mg per hour. At a considerably lower RH of 37.1%, the evaporation rate further escalated, with 192 mg of water evaporating per hour. Intriguingly, these transpiration processes actively modulate the environmental humidity, demonstrating the artificial

plant's capacity to regulate relative humidity. Specifically, under high humidity conditions, the increase in surrounding humidity was minimal, whereas significant increases were observed under lower humidity levels. This phenomenon underscores the potential of our artificial plant system to adaptively manage environmental humidity through its transpiration dynamics.

To assess the water absorption capacity of the system, which incorporates hygroscopic branches and trunk, red ink was introduced at the base (Figure 4c). To isolate the capillary force as the sole mechanism of fluid movement, the experiment was conducted under conditions of 100% RH, effectively eliminating the influence of transpiration. The capillary action enabled the ink to ascend against gravity. Notably, the ink progressively moved through the system, reaching individual leaves and eventually each biosolar cell in 180 min. This experiment demonstrates the effectiveness of capillary forces in distributing fluids within the integrated system.

2.4. Enhanced Indoor Air Quality

In this study, we used a controlled environment chamber measuring 16″ × 11″ × 12″, equipped with adjustable temperature, humidity, and light settings, to assess the CO_2 capture and O_2 generation capabilities of our artificial plant. This setup aimed to evaluate the potential for indoor air quality improvement. Along with a continuous supply of BG-11 nutrients, the chamber was subjected to a diurnal cycle with 12 h periods of light and darkness, maintaining temperature and humidity at set levels, with light intensity capped at 700 lux. Initially, the chamber was filled with CO_2 gas to a concentration of ≈5000 ppm. The nanoparticle-enhanced, leaf-inspired porous structure of the artificial plant without cyanobacteria as a living biocatalyst demonstrated significant CO_2 absorption capabilities, reducing the CO_2 levels to 1500 ppm solely through physical adsorption (**Figure 5a** (i)). This reduction is primarily attributed to van der Waals forces which trap CO_2 molecules on the material's surface.[30] However, once saturated, the structure did not exhibit further CO_2 capture when reintroduced with CO_2, indicating a capacity limit in the absence of active biological mechanisms. Interestingly, O_2 levels continuously declined, particularly upon the reintroduction of CO_2. Elevated indoor CO_2 concentrations can exacerbate O_2 depletion by displacing available O_2, especially in closed environments influenced by high occupancy and activities such as cooking and heating. This phenomenon is crucial, considering that decreased indoor O_2 levels can lead to serious health issues, including chronic obstructive pulmonary diseases and other respiratory complications.[31] The critical importance of O_2, particularly highlighted during the COVID-19 pandemic for patient care,[32] underscores the necessity of maintaining adequate indoor air quality. When cyanobacteria were incorporated into the system, not only was a CO_2 reduction observed, but also an enhancement in O_2 production (Figure 5a (ii)). The reintroduction of CO_2 was effectively mitigated, reducing the concentration to as low as 500 ppm, well below the commonly recommended indoor level of 1000 ppm. This represents a significant enhancement in CO_2 capture efficiency, achieving over 90% reduction compared to ≈10% typically observed in natural plants.[33] Concurrently, O_2 levels increased steadily, even accounting for cyanobacterial respiration and cathodic reactions. Moreover, distinct fluctuations in temperature and humidity were observed during the diurnal cycles, indicative of active bacterial metabolic reactions, in contrast to the stability observed in the non-biological setup. Over 150 h of diurnal cycles, there was significant growth and reproduction among the cyanobacteria, resulting in a marked increase in their population (Figure 5b). However, this population growth eventually stabilized because of limitations in available light, gas, and nutrients. This chapter demonstrates the profound potential of integrating cyanobacteria into artificial plant systems for dynamic indoor air quality management, offering a substantial improvement over traditional methods and natural plant capabilities.

2.5. Power Production

As a pivotal CO_2 capture and utilization (CCU) technology for next-generation smart cities and large-scale greenhouse gas mitigation, microalgae and cyanobacteria have gained significant attention.[34,35] These organisms capture, store, and convert CO_2 into biomass and valuable products via photosynthesis. O_2 generation, discussed in the previous chapter, represents one of the utilization pathways. Using these biological entities as living catalysts, the biosolar cell presents a sustainable and economically viable CCU method, transforming captured CO_2 into bioelectricity. Although its power generation capacity is not suited for large-scale, high-power demands, it is perfectly tailored for low-power applications indoors, powered effectively by a stack of multiple biosolar cells. Our research group pioneered miniaturized biosolar cell techniques applicable to various devices including the Internet of Things (IoT), surveillance robots, and sensors.[36–39] Here, we leverage this technology to develop an artificial plant that enhances indoor carbon capture while concurrently generating O_2 and substantial electrical power. Each biosolar cell achieves an open circuit voltage (OCV) of 0.25 V and a maximum power density of 9 μW cm^{-2} (**Figure 6a**). By connecting five biosolar cells in series within each leaf, we achieve an OCV of 1.0 V and a maximum power of 46 μW. Significantly, when these leaves are connected in series within the artificial plant structure, the system produces an OCV of 2.7 V and a maximum power of 140 μW, which is sufficient to power portable electronics. A single artificial leaf can power a thermometer, while the entire plant can run a desktop light-emitting diode (LED), showcasing the potential of our artificial plant as a reliable power source for indoor applications, simultaneously improving air quality as demonstrated in the previous chapter.

We also investigated the effect of CO_2 concentration on electrical performance (Figure 6b). A single artificial leaf was tested in a chamber with an initial CO_2 concentration of 5000 ppm. The initial maximum power was ≈46 μW with a maximum current of 160 μA. As the experiment progressed and CO_2 concentration decreased to 3000 ppm, the electrical performance notably increased to 65 μW and 420 μA. That marked enhancement was attributed to the increased electricity production achieved through optimized photosynthesis at high CO_2 concentrations. However, further reductions in CO_2 concentration to 2300 ppm and then 1900 ppm over time led to a gradual decline in electrical output. This decline is primarily because of the limiting effect of lower

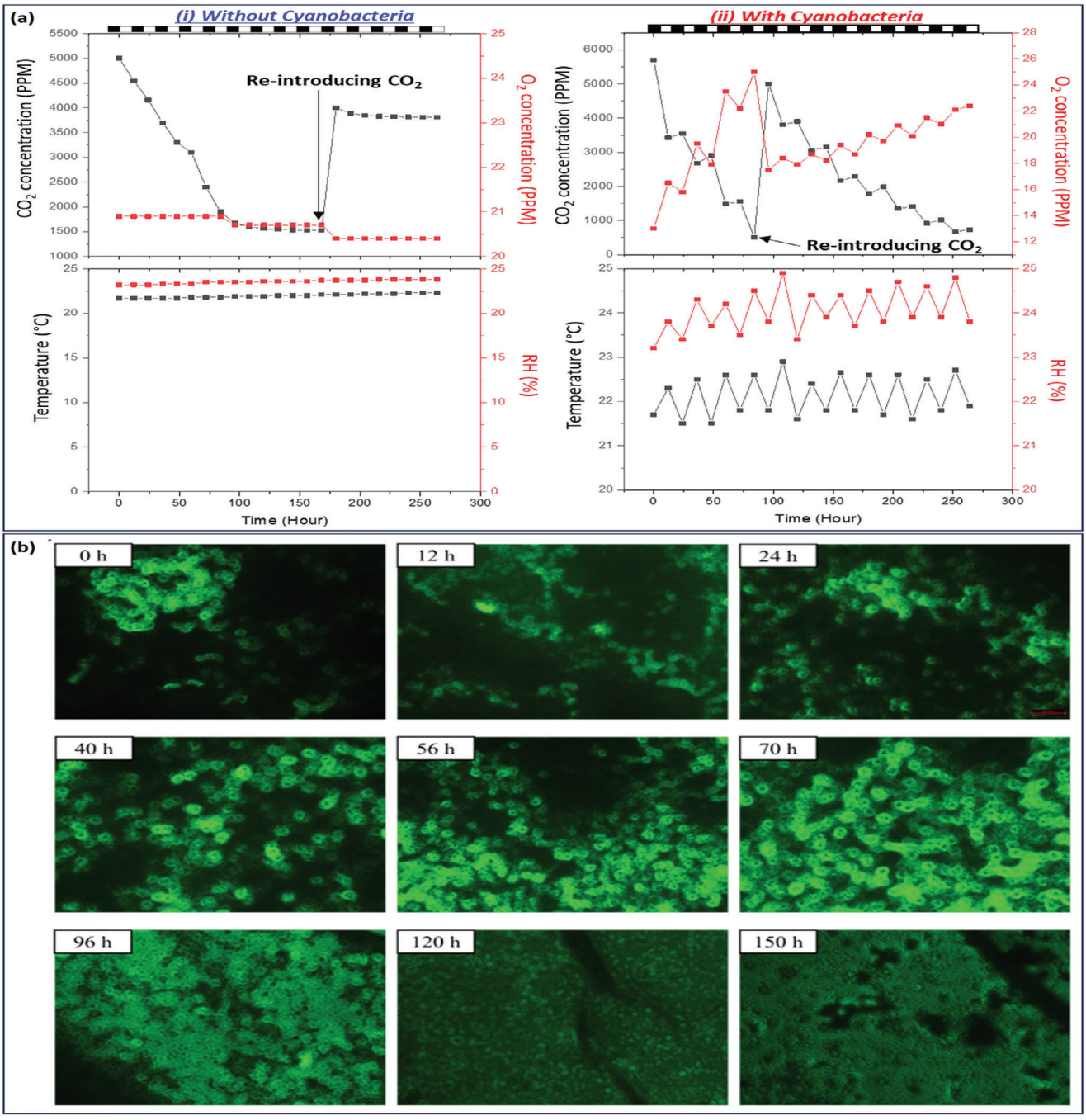

Figure 5. Cyanobacterial artificial plant for enhanced indoor quality. a) Measurements of CO_2 concentration, O_2 concentration, temperature, and humidity in an experimental chamber featuring our artificial plant (i) without and (ii) with cyanobacteria was placed. b) Time-lapse fluorescence images showing cyanobacterial growth and reproduction in the artificial plant.

CO_2 concentrations on cyanobacterial photosynthesis. Additionally, increasing O_2 concentrations may induce oxidative stress, damaging cellular components and disrupting key metabolic pathways.[40] Elevated oxygen levels can also interfere with extracellular electron transfer, significantly impairing the overall power performance of the system.[41] This intricate relationship between gas concentrations and electrical output underlines the complex interdependencies within the biosolar cell system and highlights the challenges and considerations necessary for optimizing CCU technologies in indoor environments.

3. Future Direction

We anticipate that our artificial plant can be effortlessly installed in any indoor environment in a cost-effective, maintenance-free, and eco-friendly manner. Since it is power-free and

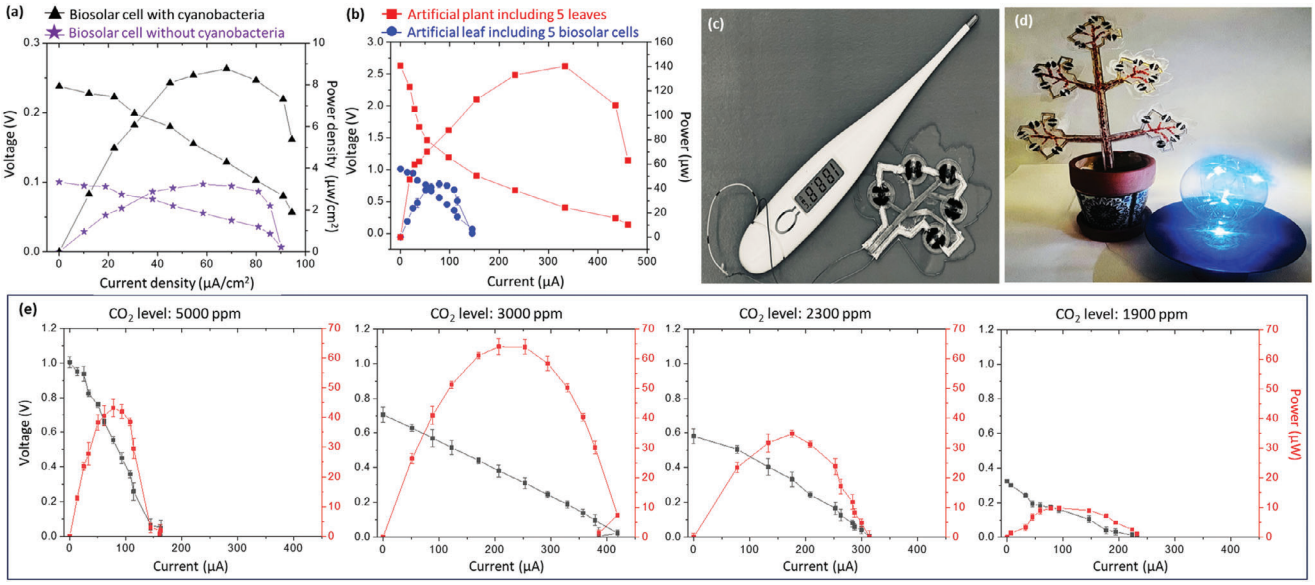

Figure 6. Power generation. a) Polarization curves and power densities from a biosolar cell with and without cyanobacteria. b) Polarization curves and power outputs from an artificial plant and an artificial leaf. c) A photo of the artificial leaf powering a digital thermometer. d) A photo of the artificial plant powering a desktop light-emitting diode (LED). e) Polarization curves and power outputs from an artificial leaf during CO_2 reduction.

self-sustaining, no external energy sources or accessory components are required. However, additional studies are necessary to further refine its practical applications. Here, the long-term operation necessary for ideal and permanent improvements in indoor air quality was not achieved. The use of a single bacterial species may limit long-term bacterial viability, suggesting that engineered co-culture communities might be more advantageous for sustained operation.[42] Additionally, exploring the genetic engineering of bacteria could enhance performance. Moreover, minimizing maintenance, which can be achieved through optimized water and nutrient delivery systems, is crucial for practical application. Regarding power performance, generating higher power output is essential for more practical indoor applications, such as charging a cellphone. It is anticipated that a minimum output of more than 1 mW is necessary. To accomplish this, further improvements in materials and device structures are required. Increasing the compactness and number of biosolar cells could significantly enhance power output. Additionally, integrating energy storage solutions, such as lithium-ion batteries and supercapacitors, should be considered to make the system more effective and versatile for real-world applications. These future directions will pave the way for cyanobacterial artificial plants to become a viable technology for indoor environmental management and sustainable energy.

4. Conclusion

This work develops a cyanobacteria-activated artificial plant, which comprises artificial leaves connected to a stem through microfluidic channels and electrical pathways. Cyanobacteria harness solar energy to transform CO_2 and water into O_2, thereby enhancing indoor air quality. Concurrently, excess electrons released from the photosynthesis in cyanobacteria are harnessed as a source of energy for low-power applications. The electricity generated is captured by an integrated biosolar cell that includes a cyanobacteria-embedded anode and a cathode, separated by an ion exchange membrane. The structural basis of the leaves and plant stems incorporates microporous hygroscopic hydrogels, which facilitate continuous water and nutrient supply to individual leaves via capillary forces and transpiration. The hydrogels are further enhanced with Fe_2O_3 NPs, which not only augment CO_2 capture and light absorption but also improve light harvesting and extracellular electron transfer rates in cyanobacteria, acting as effective light absorbers and conductive conduits, respectively. The artificial plant, integrating five leaves each with five serially connected biosolar cells, achieves a substantial reduction in indoor CO_2 levels—from 5000 to 500 ppm—and a corresponding increase in O_2 levels—from 13.2 to 22.9 ppm. This setup also generates a significant power density of 140 μW cm^{-2}, demonstrating its potential as a dual-function system for improving air quality and providing sustainable energy.

5. Experimental Section

Cultivation of Cyanobacteria: The cyanobacterial strain *Synechocystis* sp. PCC 6803 was revived from an −80 °C glycerol stock culture. The culture was inoculated into 15 mL of BG-11 medium and maintained under gentle shaking conditions, following a 12 h light/dark cycle. The BG-11 medium was prepared with the following composition per liter of distilled water: 1.5 g of $NaNO_3$, 40 mg of K_2HPO_4, 75 mg of $MgSO_4$, 36 mg of $CaCl_2$, 1 mg of EDTA, and 6 mg each of citric acid and ferric ammonium citrate. Cultivation took place in a chamber controlled by fluorescent lighting at a consistent temperature of 30 ± 2 °C, with continuous aeration and illumination for two weeks. The growth of the culture was periodically assessed by measuring the optical density at 600 nm (OD600), which reached a final value of 1.2, indicating successful proliferation.

Synthesis of Anodic and Cathodic Materials: A leaf-inspired Fe_2O_3 decorated rGO hydrogel was synthesized using a hydrothermal method. Initially, 50 mg of GO was dissolved in 25 mL of distilled water (DIW) and sonicated for 10 min to ensure a homogeneous mixture. Subsequently,

20 mg of $FeSO_4 \cdot 7H_2O$ was added and the solution was stirred continuously for 1 h at room temperature. The resultant mixture was then transferred to a Teflon-lined autoclave and subjected to hydrothermal treatment at 200 °C for 22 h. During this process, the oxygen-containing functional groups in the GO were reduced, transforming it into rGO with enhanced electrical conductivity. Concurrently, Fe_2O_3 NPs were synthesized in situ within the hydrothermal environment. These NPs became uniformly dispersed throughout the rGO network, forming a composite hydrogel with improved structural and functional properties. Following synthesis, the autoclave was allowed to cool to room temperature. The hydrogel was then washed three times with DIW to remove any residual reactants and byproducts, ensuring the purity of the final product. To finalize the preparation, the hydrogel was freeze-dried for 36 h using a FreeZone Plus 2.5 Liter Cascade Benchtop Freeze Dry System, effectively removing all residual moisture.

For the cathodic part of the biosolar cells, an AC hydrogel decorated with Pd NPs was prepared. To begin, 100 mg of AC powder was dissolved in 45 mL of DIW and vigorously stirred for 2 h. Subsequently, 35 mg of Palladium (II) chloride was added to the mixture, which was stirred for an additional hour. This mixture then underwent hydrothermal treatment under the same conditions as the anodic structure, ensuring consistency in the processing conditions across both electrodes. Finally, to assemble the biosolar cells, a solution of PEDOT:PSS and glycerol was prepared and mixed with the anode and cathode materials. This mixture was carefully injected into the designated anodic and cathodic regions to complete the cell assembly.

Synthesis of Ion Exchange Membrane Material: Initially, 2 grams of chitosan powder were dissolved in 100 mL of 2% (w/v) acetic acid solution under constant stirring to ensure thorough dissolution. This step is crucial for the uniformity of the membrane matrix. Subsequently, 100 µL of 2.5% (v/v) glutaraldehyde solution was incorporated into the chitosan solution as a crosslinking agent. The inclusion of glutaraldehyde is critical as it facilitates the formation of stable crosslinks within the chitosan structure, which is rich in amino groups. These amino groups are instrumental in promoting ion exchange with oppositely charged ions. The cross-linking process conferred by glutaraldehyde significantly enhances the membrane's stability and selectivity in ion transport, effectively allowing the passage of certain ions while obstructing others.[43] These properties render the chitosan-based membrane highly suitable for applications as an ion exchange membrane, ensuring efficient and selective ion separation critical in various industrial and research applications.

Synthesis of Hygroscopic Gelatin-Chitosan Hydrogel: The preparation of the hygroscopic hydrogel commenced with the blending of chitosan and gelatin in a ratio of 1:2 in a 2 wt% acetic acid solution within 50 ml of DIW. This mixture was stirred continuously for 4 h at 40 °C to achieve a homogeneous solution. Subsequently, the solution was degassed under vacuum for 2 h to eliminate any entrapped air bubbles, enhancing the uniformity of the final product. To facilitate cross-linking, 0.25 wt% glutaraldehyde solution was added to the gelatin-chitosan mixture. This step is critical as it promotes the formation of stable bonds between the polymer chains of chitosan and gelatin, significantly enhancing the structural integrity of the hydrogel. Following the addition of glutaraldehyde, the mixture was freeze-dried at −60 °C for 24 h. The freeze-drying is essential as it sublimates the water content directly from the solid phase to the gas phase, thereby creating a porous structure within the hydrogel. The hygroscopic properties of the hydrogel are primarily attributed to the presence of hydrophilic functional groups—namely amino and hydroxyl groups—within the chitosan and gelatin. These groups exhibit a strong affinity for water molecules, enabling the scaffold to efficiently absorb and retain moisture from its environment. Additionally, the porosity introduced by the freeze-drying further amplifies its moisture-absorbing capabilities. The cross-linking induced by glutaraldehyde not only reinforces the hydrogel's mechanical stability but also ensures that it remains intact and does not dissolve upon exposure to water. This combination of structural and chemical properties makes the hydrogel ideally suited for applications requiring durable and efficient water supply management.

Fabrication of Artificial Plant: The fabrication of individual leaves on a 1.6 mm thick PMMA substrate was accomplished using a laser micromachining technique, specifically employing the Universal Laser Systems VLS 3.5. This precision engineering process meticulously defines designated areas for fluidic and electrical channels, alongside the integral components of the biosolar cells. During this process, the internal circle of the biosolar cell, measuring 11 mm in diameter, was segmented into three equal parts. The cathode and anode materials were meticulously applied onto the substrate to achieve a consistent thickness of ≈1 mm. After this initial setup, the membrane separating the anode and cathode, as well as the hydrogel for the branches and stems, and silver for constructing metallic pathways, were precisely deposited using an ink-jet printing technique. This advanced method guarantees exact placement and seamless integration of the various functional materials, ensuring optimal performance and structural integrity of the device. The anodes of the individual leaves were fluidically interconnected, a design feature that ensures consistent and efficient delivery of water and nutrients to the embedded cyanobacteria. Moreover, the anodes and cathodes of each leaf were electrically connected, optimizing the electrical output and overall power performance of the system. This interconnected arrangement facilitates the effective operation of the artificial plant, enhancing its functional efficiency and the scalability of the design for larger systems.

Indoor Air Quality Measurement Setup: The artificial plant and its associated leaves were placed within an environmental test chamber (Model Tenney 90 906) to evaluate their CO_2 capture and O_2 generation capabilities under controlled environmental conditions. The experiment was structured to simulate natural diurnal cycles, consisting of 12 h of daylight and 12 h of darkness, with a constant light intensity of 700 lux during the daylight hours. Before initiating the experiment, the chamber was purged with CO_2 gas to remove other gases, including O_2 and N_2, to create a controlled atmospheric environment. Throughout the experiment, critical environmental parameters such as temperature, humidity, O_2 levels, and CO_2 levels were continuously monitored. These measurements were conducted using an indoor air quality monitor equipped with data logging capabilities (Model: 800 049, Sper Scientific) and an additional oxygen sensor (AirRadio Combustible Gas Leak Detector Portable). This comprehensive monitoring allowed for precise data collection and analysis of the artificial plant's performance in terms of gas exchange under the specified test conditions.

Electrochemical Measurement Setup: The electrochemical characterization of the anodic and cathodic materials was conducted using advanced analytical techniques, including CV, EIS, and LSV. These tests were performed using a Squidstat Plus potentiostat from Admiral Instruments. Experiments were carried out in a 0.5 M KCl buffer solution employing a screen-printed electrode supplied by Metrohm, USA. The CV method provided insights into the redox characteristics and charge transfer capabilities of the materials. EIS was used to assess the impedance properties across a range of frequencies, thereby elucidating the materials' resistance and capacitive behaviors. LSV was used to further evaluate the electrochemical kinetics and reaction mechanisms at the electrode surfaces. The data collected from these electrochemical tests were critical for assessing the performance parameters of the materials, offering a comprehensive understanding of their electrochemical properties within the biosolar cell system.

Electrical Measurement Setup: The electrical performance of the biosolar cells was rigorously assessed using a Data Acquisition System (Model DI-4108U, DataQ, USA). The system facilitated continuous monitoring of the electrical outputs across various external resistors, ranging from no resistance to 0.35 kΩ. This method allowed for the precise measurement of voltage across these resistors, which is essential for constructing polarization curves and determining power outputs. Furthermore, to provide a standardized basis for comparison and analysis, the power and current densities were normalized to the surface area of the anode. This normalization is critical as it accounts for variations in anode size and ensures that the performance data are directly comparable across different biosolar cell setups.

Statistical Analysis: Statistical analysis was conducted on experimental data obtained from a minimum of three identical trials. The results were presented as the mean ± standard error of the mean for these replicates, providing a robust measure of variability and accuracy.

Supporting Information

Supporting Information is available from the Wiley Online Library or from the author.

Acknowledgements

This research was supported by funding from the Office of Naval Research (Grant #: N00014-21-1-2412). The authors are grateful to the Analytical and Diagnostic Laboratory at SUNY-Binghamton for providing access to their facilities. During the preparation of this manuscript, the authors employed ChatGPT to identify and correct grammatical inaccuracies. After this assistance, the authors carefully reviewed and revised the manuscript to ensure accuracy and clarity. The authors accept full responsibility for the content of this publication.

Conflict of Interest

The authors declare no conflict of interest.

Data Availability Statement

The data that support the findings of this study are available from the corresponding author upon reasonable request.

Keywords

artificial plants, biosolar cells, CO_2 capture and utilization, cyanobacteria, indoor air quality, synechocystis sp. PCC 6803

Received: June 6, 2024
Revised: July 19, 2024
Published online:

[1] L. R. López, P. Dessi, A. Cabrera-Codony, L. Rocha-Melogno, B. Kraakman, V. Naddeo, M. D. Balaguer, S. Puig, *Sci. Total Environ.* **2023**, *856*, 159088.
[2] H. Tian, L. Zhu, J. Ni, T. Wei, P. Wang, H. Xiao, X. Chen, *Mater. Today Sustainability* **2023**, *22*, 100369,.
[3] T. M. Mata, A. A. Martins, C. S. C. Calheiros, F. Villanueva, N. P. Alonso-Cuevilla, M. F. Gabriel, G. V. Silva, *Environments* **2022**, *9*, 118.
[4] S. D. Lowther, S. Dimitroulopoulou, K. Foxall, C. Shrubsole, E. Cheek, B. Gadeberg, O. Sepai, *Environments* **2021**, *8*, 125.
[5] D. B. Collins, D. K. Karmer, *Environ. Sci. Technol.* **2021**, *55*, 12172.
[6] S. Hattori, T. Iwamatsu, T. Miura, F. Tsutsumi, N. Tanaka, *Sensors* **2022**, *22*, 7331.
[7] T. M. Gür, *Prog. Energy Combust. Sci.* **2022**, *89*, 100965.
[8] S. Castro-Pardo, S. Bhattacharyya, R. M. Yadav, A. P. de Carvalho Teixeira, M. A. C. Mata, T. Prasankumar, M. A. Kabbani, M.d G. Kibria, T. Xu, S. Roy, P. M. Ajayan, *Mater. Today* **2022**, *60*, 227.
[9] X. An, P. Wang, X. Ma, X. Du, X. Hao, Z. Yang, *Carbon Resour. Convers.* **2023**, *6*, 85.
[10] J. Godin, W. Liu, S. Ren, C. C. Xu, *J. Environ. Chem. Eng.* **2021**, *9*, 105644.
[11] S. A. Theofanidis, A. N. Antzaras, A. A. Lemonidou, *Curr. Opin. Chem. Eng.* **2023**, *39*, 100902.
[12] J. Yuan, X. Song, X. Yang, C. Yang, Y. Wang, G. Deng, Z. Wang, J. Gao, *Environ. Chem. Lett.* **2023**, *21*, 2559.
[13] T. M. Mata, G. M. Oliveria, H. Monteiro, G. V. Silva, N. S. Caetano, A. A. Marins, *Int. J. Environ. Res. Public Health* **2021**, *18*, 8472.
[14] R. El-Tanbouly, Z. Hassan, S. El-Messeiry, *Front. Mol. Biosci.* **2021**, *8*, 709395.
[15] R. Kumar, V. Verma, M. Thakur, G. Singh, B. Bhargava, *Air Qual., Atmos. Health* **2023**, *16*, 1501.
[16] K. Chuang, C. Lee, S. Wang, I. Liu, H. Chuang, K. Ho, *Indoor Air* **2023**, 1558047.
[17] A. J. McCormick, P. Bombelli, A. M. Scott, A. J. Philips, A. G. Smith, A. C. Fisher, C. J. Howe, *Energy Environ. Sci.* **2011**, *4*, 4699.
[18] P. Bombelli, R. W. Bradley, A. M. Scott, A. J. Philips, A. J. McCormick, S. M. Cruz, A. Anderson, K. Yunus, D. S. Bendall, P. J. Cameron, J. M. Davies, A. G. Smith, C. J. Howe, A. C. Fisher, *Energy Environ. Sci.* **2011**, *4*, 4690.
[19] A. Elhadad, S. Choi, *Adv. Eng. Mater.* **2023**, *25*, 2301137.
[20] A. Elhadad, L. Liu, S. Choi, *J. Power Sources* **2022**, *535*, 231487.
[21] R. Al-Gaashani, A. Najjar, Y. Zakaria, S. Mansour, M. A. Atieh, *Ceram. Int.* **2019**, *45*, 14439.
[22] L. Han, S. Dong, E. Wang, *Adv. Mater.* **2016**, *28*, 9266.
[23] Y. Gao, M. Mohammadifar, S. Choi, *Adv. Mater. Technol.* **2019**, *4*, 1970039.
[24] M. Wang, X. Qin, K. Jiang, Y. Dong, M. Shao, W. Cai, *J. Phys. Chem.* **2017**, *121*, 3416.
[25] B. J. Kramer, J. G. Jankowiak, D. Nanjappa, M. J. Harke, C. J. Gobler, *Front. Microbiol.* **2022**, *13*, 955032.
[26] G. Markou, D. Vandamme, K. Muylaert, *Water Res.* **2014**, *65*, 186.
[27] E. Pulieri, V. Chiono, G. Ciardelli, G. Vozzi, A. Ahluwalia, C. Domenici, F. Vozzi, P. Giusti, *J. Biomed. Mater. Res., Part A* **2008**, *86*, 311.
[28] A. J. McElrone, B. Choat, G. A. Gambetta, C. R. Brodersen, *Nat. Edu. Knowledge* **2013**, *4*, 6.
[29] H. F. Thut, *Am. J. Bot.* **1938**, 589.
[30] S. Chowdhury, R. Balasubramanian, *J. CO2 Util.* **2016**, *13*, 50.
[31] S. K. Sameer, P. Eswaran, *IOP Conf. Series: Mater. Sci. Eng.* **2020**, *912*, 042054.
[32] N. Bhat, V. Moses, N. Chetan, *Hygiene Environ. Health Adv.* **2023**, *6*, 100048.
[33] M. M. Suhaimi, A. M. Leman, A. Afandi, A. Hariri, A. F. Idris, S. N. Mohd Dzulkifli, P. Gani, *MATEC Web Conf.* **2017**, *103*, 05004.
[34] S. Li, X. Li, S. Ho, *Sep. Purif. Technol.* **2022**, *291*, 120951.
[35] S. K. Bhatia, R. K. Bhatia, J. Jeon, G. Kumar, Y. Yang, *Renewable Sustainable Energy Rev.* **2019**, *110*, 143.
[36] A. Elhadad, S. Choi, *J. Power Sources* **2023**, *581*, 233501.
[37] L. Liu, S. Choi, *Biosens. Bioelectron.* **2021**, *177*, 112970.
[38] M. Mohammadifar, M. Tahernia, S. Choi, *Nano Energy* **2020**, *72*, 104668.
[39] L. Liu, S. Choi, *Lab Chip* **2017**, *17*, 3817.
[40] S. H. Liu, S. L. Tsai, Y. R. Lai, C. W. Lin, Y. W. Huang, *Chemosphere* **2021**, *278*, 130390.
[41] C. Xu, K. Poon, M. M. Choi, R. Wang, *Environ. Sci. Pollut. Res.* **2015**, *22*, 15621.
[42] L. Liu, M. Mohammadifar, A. Elhadad, M. Tahernia, Y. Zhang, W. Zhao, S. Choi, *Adv. Energy Mater.* **2021**, *11*, 2100713.
[43] B. Feketeföldi, B. Cermenek, C. Spirk, A. Schenk, C. Grimmer, M. Bodner, M. Koller, V. Ribitsch, V. Hacker, *J. Membr. Sci. Technol.* **2016**, *6*, 145.